

Broadband source-surrounded cloak for on-chip antenna radiation pattern protection

HANCHUAN CHEN,¹ FEI SUN,^{1,*} YICHAO LIU,¹ HONGMING FEI,¹ ZHIHUI CHEN¹

¹Key Lab of Advanced Transducers and Intelligent Control System, Ministry of Education and Shanxi Province, College of Physics and Optoelectronic Engineering, Taiyuan University of Technology, Taiyuan 030024, China

*sunfei@tyut.edu.cn

Received XX Month XXXX; revised XX Month, XXXX; accepted XX Month XXXX; posted XX Month XXXX (Doc. ID XXXXX); published XX Month XXXX

As the frequency range of electromagnetic wave communication continues to expand and the integration of integrated circuits increases, electromagnetic waves emitted by on-chip antennas are prone to scattering from electronic components, which limits further improvements in integration and the protection of radiation patterns. Cloaks can be used to reduce electromagnetic scattering; however, they cannot achieve both broadband and omnidirectional effectiveness simultaneously. Moreover, their operating modes are typically designed for scenarios where the source is located outside the cloak, making it difficult to address this problem. In this work, we propose a dispersionless air-impedance-matched metamaterial over the 2-8 GHz bandwidth that achieves an adjustable effective refractive index ranging from 1.1 to 1.5, with transmittance maintained above 93%. Based on this metamaterial, we introduce a broadband source-surrounded cloak that can guide electromagnetic waves from a broadband source surrounded by the cloak in any propagation direction to bypass obstacles and reproduce the original wavefronts outside the cloak. Thereby protecting the radiation pattern from distortion due to scattering caused by obstacles. Our work demonstrates significant potential for enhancing the integration density of integrated circuits and improving the operational stability of communication systems.

Improving electromagnetic wave emission efficiency has become a critical technological objective with diverse applications. In particular, on-chip communication systems benefit from it, resulting in enhanced signal quality and increased transmission reliability [1–3]. However, as the component integration of on-chip communication systems continues to increase and the communication frequency bands expand, the electromagnetic waves emitted by on-chip antennas are prone to scattering by electronic components/metallic electronic components [4–6]. This scattering will cause distortion in the radiation pattern, ultimately leading to reduced electromagnetic wave emission efficiency. To balance electromagnetic wave emission efficiency, further improvement in the integration of on-chip

communication systems has been limited. Traditional cloaks can be applied around electronic components to reduce their scattering of incident waves from the outside [7–9]. In recent years, an increasing number of invisibility mechanisms and methods have been proposed. Notable research works in this field include cloaks based on transformation optics [10–13], cloaks based on optical conformal transformation [14–16], and cloaks based on scattering-cancellation [17–20] *et al.* However, current cloaks are affected by two critical problems that limit their application in protecting the radiation patterns of on-chip sources within highly integrated on-chip communication systems. First, there is a significant bandwidth limitation. Most full-space cloaks operate only at single frequencies or narrow frequency bands [21–23]. Although directionally restricted cloaks [24,25] or carpet cloaks may achieve broadband operation [26–28], they are not suitable for protecting the radiation patterns of on-chip sources or antennas. Second, all traditional cloaks are designed for electromagnetic waves incident from the outside to encounter concealed regions, but they do not address scenarios where electromagnetic waves generated by internal sources propagate outward and encounter concealed regions containing strong electromagnetic scatterers. Therefore, there is still a lack of a cloak that allows electromagnetic waves emitted in any propagation direction to bypass obstacles without scattering and operates across a broadband frequency range, thus protecting the radiation patterns of on-chip sources/antennas from distortion caused by surrounding electronic components.

In this work, a dispersionless air-impedance-matched metamaterial (AIMM) operating over the 2-8 GHz bandwidth is proposed, achieving an adjustable effective refractive index ranging from 1.1 to 1.5. This adjustability is achieved by adjusting the dielectric mixing ratio m , while maintaining a transmittance t above 93% across the entire bandwidth. We further propose a broadband source-surrounded cloak (SSC) based on AIMM for on-chip radiation pattern protection. The SSC operates with a bandwidth of 6 GHz centered at $f_0 = 5$ GHz ($\lambda_0 = 60$ mm). As illustrated in Fig. 1(a), the SSC fundamentally differs from traditional cloaks by surrounding the source rather than the scatterer.

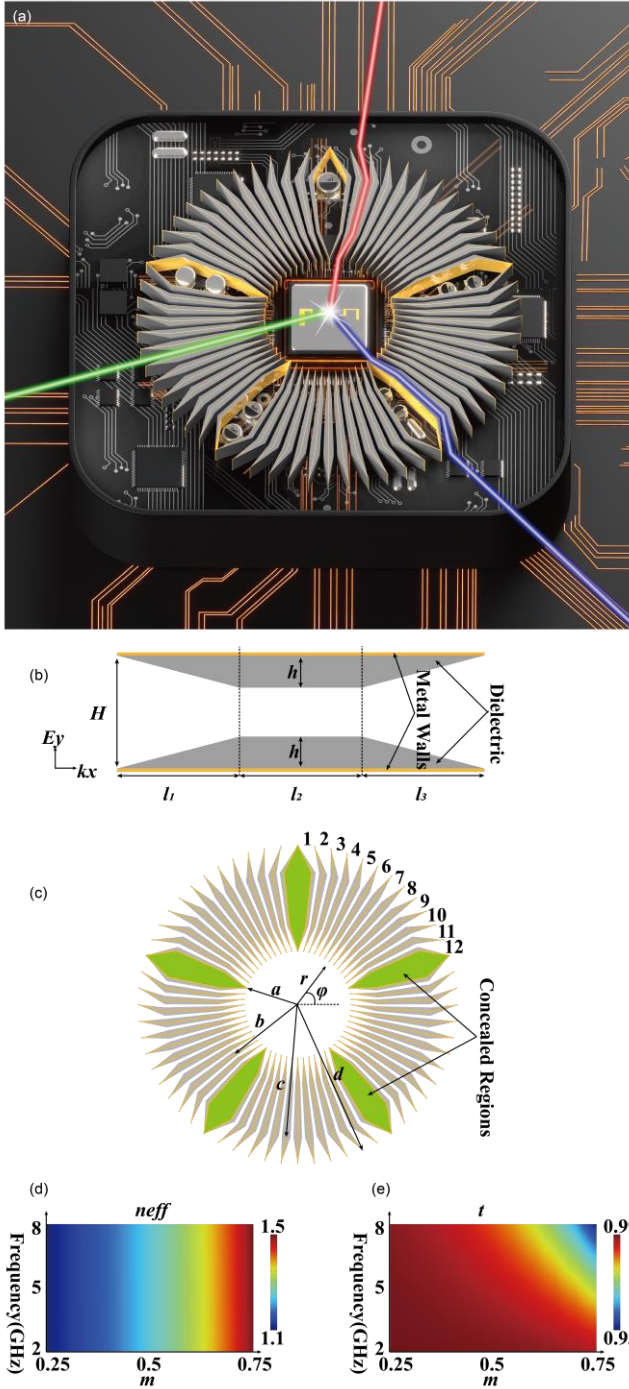


Fig. 1. SSC based on AIMM. (a) The schematic view of SSC applied to on-chip communication system. It demonstrates the on-chip antenna surrounded by SSC, with obstacles like electronic components that can scatter electromagnetic waves placed in the concealed regions of SSC. The electromagnetic waves emitted by the on-chip antenna in any propagation direction are guided around the obstacles by SSC and exit without distortion. (b) The structural schematic diagram of AIMM. The yellow lines represent metal walls, and the gray areas are dielectric regions. (c) The structural schematic diagram of SSC. The green areas represent the concealed regions. (d) Effective refractive index n_{eff} as a function of $m = 2h/H$ and the frequency. (e) Transmittance t as a function of $m = 2h/H$ and the frequency. In (d) and (e), $l_1 = 0.02\lambda_0$, $l_2 = 0.02\lambda_0$, $l_3 = 0.02\lambda_0$, $H = 0.02\lambda_0$, and the relative permittivity of dielectric regions $\epsilon_{rd} = 10$.

Electronic components can be placed within the concealed regions, while broadband electromagnetic waves emitted omnidirectionally from the source are guided by the SSC to bypass the components without scattering. Crucially, the electromagnetic waves fully reproduce their original wavefronts after exiting the cloak.

Fig. 1(b) details the structure of the AIMM, comprising top and bottom metal walls (treated as perfect electric conductor boundaries at microwave frequencies) sandwiching two symmetrical dielectric regions with relative permittivity ϵ_{rd} . The AIMM operates effectively solely for transverse magnetic (TM) waves, and accordingly, this work is confined to TM-polarized electromagnetic phenomena. The AIMM, with total height H , is partitioned along the k_x direction into three functional sections: l_1 and l_3 serving as impedance-matching sections, flanking the central l_2 section, which is the main contributing region of the effective refractive index n_{eff} . The dielectric thickness gradually increases from 0 at the outer boundaries to a maximum thickness h at the l_2 interfaces, maintaining a constant height h throughout the l_2 section. The effective refractive index n_{eff} of the AIMM is controlled by adjusting the dielectric mixing ratio $m = 2h/H$. The quantitative relationship is expressed as:

$$n_{eff} = \frac{\int_0^{l_1} \sqrt{\frac{\epsilon_0 \epsilon_{rd}}{\epsilon_0 \left(\frac{m}{l_1} k_x\right) + \epsilon_{rd} \left(1 - \frac{m}{l_1} k_x\right)}} dk_x + \sqrt{\frac{\epsilon_0 \epsilon_{rd}}{\epsilon_0 m + \epsilon_{rd} (1-m)}} \cdot l_2 + \int_0^{l_3} \sqrt{\frac{\epsilon_0 \epsilon_{rd}}{\epsilon_0 \left(\frac{m}{l_3} k_x\right) + \epsilon_{rd} \left(1 - \frac{m}{l_3} k_x\right)}} dk_x}{L}, \quad (1)$$

where ϵ_0 represents the relative permittivity of air (approximated as 1 at microwave frequencies), and $L = l_1 + l_2 + l_3$ represents the total unit cell length along the k_x -direction. As shown in Figs. 2(d) and (e), the effective refractive index n_{eff} and transmittance t of the AIMM are plotted across the 2-8 GHz under the parameters $l_1 = 0.02\lambda_0$, $l_2 = 0.02\lambda_0$, $l_3 = 0.02\lambda_0$, $H = 0.02\lambda_0$, and $\epsilon_{rd} = 10$ (e.g., Al_2O_3 [29]), with the dielectric mixing ratio m increasing from 0.25 to 0.75. The results reveal that the effective refractive index n_{eff} of the AIMM varies continuously from 1.1 to 1.5, while the structure exhibits dispersionless characteristics over the 2-8 GHz bandwidth, with the transmittance t remaining above 93%.

Fig. 1(c) illustrates the SSC constructed from a series of AIMM within a cylindrical coordinate system. Electromagnetic waves emitted omnidirectionally from the SSC surrounded source are guided by the AIMM array to bypass obstacles while precisely reproducing their original wavefronts at the outside of SSC. Using fivefold rotational symmetry, we detail the design of a 72° sector (1/5 of the full structure), with identical remaining sectors generated via rotational duplication. First, transform the AIMM into cylindrical coordinates by converting k_x to r and E_y to ϕ . As an example, set $a = 0.5\lambda_0$, $b = 0.75\lambda_0$, $c = 1.25\lambda_0$, and $d = 1.5\lambda_0$. The angle H occupied by each channel linearly decreases from 6° at a to 5° at b , remains at 5° from b to c , and then linearly increases back to 6° from c to d . The selection of H must satisfy the subwavelength condition at the highest operating frequency. Five hexagonal concealed regions surrounded by metal walls can be generated via rotational symmetry (the green areas in Fig. 1(c)). Since the lengths of the channels are inconsistent, to ensure the wavefront shapes remains

unchanged, the dielectric mixing ratio m is adjusted to equalize the optical path length d_i ($i = 1, 2, 3, \dots, 12$, representing the channel number) through the condition:

$$d_i = n_{\text{eff}}^i L_i = \text{constant}. \quad (2)$$

The optical path length d_i for all channels is set to $3/2\lambda_0$. According to Eqs. (1) and (2), the dielectric mixing ratio m and structural parameters l_1 , l_2 , and l_3 of the AIMMs in each channel are calculated and summarized in Table 1.

Table 1. The AIMM Parameters for the SSC in Fig. 1(c)

Channel Number	m	l_1 (mm)	l_2 (mm)	l_3 (mm)
1	0.7054	15.411	30.000	16.957
2	0.7170	15.278	30.000	16.341
3	0.7262	15.170	30.000	15.831
4	0.7332	15.088	30.000	15.438
5	0.7379	15.034	30.000	15.170
6	0.7402	15.006	30.000	15.034
7	0.7402	15.006	30.000	15.034
8	0.7379	15.034	30.000	15.170
9	0.7332	15.088	30.000	15.438
10	0.7262	15.170	30.000	15.831
11	0.7170	15.278	30.000	16.341
12	0.7054	15.411	30.000	16.957

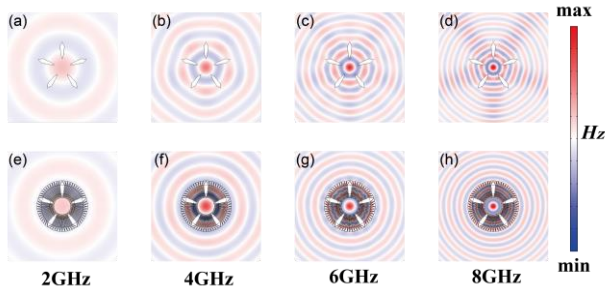


Fig. 2. Normalized magnetic field distribution at 2, 4, 6, 8 GHz from 2D numerical simulation with a centered magnetic current point source. (a)-(d) The reference. (e)-(h) The cloak surrounding the source.

Fig. 2 presents numerical simulations of the SSC conducted with COMSOL Multiphysics (License #9406999) with its two-Dimensional (2D) Wave Optics module. The simulation domain is limited to a $6.5\lambda_0 \times 6.5\lambda_0$ square region surrounded by perfect matched layers of thickness $0.5\lambda_0$, centered on a 1 V magnetic point source. Figs. 2(a)-(d) show reference normalized magnetic field distributions with five PEC obstacles (matching the concealed regions geometry) surrounding the source at 2, 4, 6, 8 GHz. Strong radiation pattern distortions caused by PEC scattering are observed, exacerbating at shorter wavelengths. Figs. 2(e)-(h) demonstrate the source surrounded by SSC at 2, 4, 6, 8 GHz. Here, electromagnetic waves emitted omnidirectionally from the source are guided around the obstacles and reproduce cylindrical wavefronts at the outer boundary of SSC across the entire 6 GHz bandwidth. These results validate that the

SSC effectively protects the radiation pattern of broadband sources from scattering by obstacles, regardless of emission direction or operating frequency within the designed bandwidth.

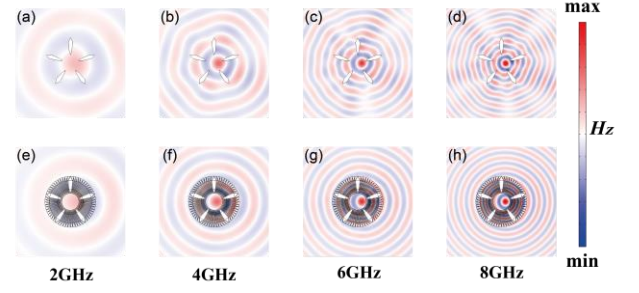


Fig. 3. Normalized magnetic field distribution at 2, 4, 6, 8 GHz from 2D numerical simulation with the magnetic current point source positioned 15 mm off-center. (a)-(d) The reference. (e)-(h) The cloak encircling the source.

To further validate the applicability of the SSC, we conduct 2D numerical simulations to verify its effectiveness when the point source is offset from the center of the SSC. As shown in Fig. 3, the magnetic point source is offset to the right by $0.25\lambda_0$ from the center. The reference normalized magnetic field distributions with five PEC obstacles (matching the concealed regions geometry) surrounding the source show significant radiation pattern distortions caused by scattering from the PEC obstacles (see Fig. 3(a)-(d)). However, when the source is surrounded by the SSC, the electromagnetic waves emitted by the source are guided around the concealed regions and reproduce cylindrical wavefronts at the outer boundary of SSC across the entire operating bandwidth, protecting the radiation pattern of broadband sources from scattering by obstacles (see Fig. 3(e)-(h)). Notably, the distribution of electromagnetic waves outside the SSC is also offset to the right by $0.25\lambda_0$ relative to the case where the source is at the center of the SSC. This demonstrates that the SSC remains effective for electromagnetic wave sources located anywhere within its inner boundary.

In conclusion, in this work, we propose a dispersionless air-impedance-matched metamaterial over the 2-8 GHz bandwidth that achieves an adjustable effective refractive index ranging from 1.1 to 1.5, with transmittance maintained above 93%. Based on the AIMM, we design an SSC which surrounds the electromagnetic wave source to create five concealed regions. TM electromagnetic waves emitted by the source in any propagation direction can be guided by the SSC to bypass the concealed regions and reproduce the original wavefronts outside the SSC at 2-8 GHz. Thus, it protects the radiation pattern from being distorted by scattering from obstacles. We further validate the applicability of its functionality. Even when the electromagnetic wave source is not strictly centered within the SSC but offset by a certain distance, the SSC still protects the radiation patterns from scattering by obstacles, and the reproduced electromagnetic waves are similarly offset by that distance. Our work demonstrates significant potential for enhancing the integration density of integrated circuits and improving the operational stability of communication systems.

Funding. This work is supported by the National Natural Science Foundation of China (Nos. 12274317, 12374277), and 2024 Postgraduate Research and Innovation Project of Shanxi Province (2024KY220).

Disclosures. The authors declare no conflicts of interest.

Data availability. The main data and models supporting the findings of this study are available within the paper. Further information is available from the corresponding authors upon reasonable request.

References

1. X. Wang, J. Han, S. Tian, D. Xia, L. Li, and T. J. Cui, "Amplification and Manipulation of Nonlinear Electromagnetic Waves and Enhanced Nonreciprocity using Transmissive Space-Time-Coding Metasurface," *Adv. Sci.* 9, 2105960 (2022).
2. W. Wang and Y. Zheng, "Wideband Gain Enhancement of a Dual-Polarized MIMO Vehicular Antenna," *IEEE Trans. Veh. Technol.* 70, 7897 (2021).
3. J. Zhang, H. Liu, Q. Wu, Y. Jin, Y. Chen, B. Ai, S. Jin, and T. J. Cui, "RIS-Aided Next-Generation High-Speed Train Communications: Challenges, Solutions, and Future Directions," *IEEE Wirel. Commun.* 28, 145 (2021).
4. Y. Liu, H. Chen, G. Zhao, and F. Sun, "On-chip omnidirectional electromagnetic-thermal cloak," *iScience* 27, 110105 (2024).
5. H. Chen, Y. Liu, F. Sun, Q. Sun, X. Wu, and R. Sun, "A Thermal-EM Concentrator for Enhancing EM Signals and Focusing Heat Fluxes Simultaneously," *Laser Photonics Rev.* 2400488 (2024).
6. Y. Liu, X. Ma, K. Chao, F. Sun, Z. Chen, J. Shan, H. Chen, G. Zhao, and S. Chen, "Simultaneously realizing thermal and electromagnetic cloaking by multi-physical null medium," *Opto-Electron. Sci.* 3, 230027 (2024).
7. J. B. Pendry, D. Schurig, and D. R. Smith, "Controlling Electromagnetic Fields," *Science* 312, 1780 (2006).
8. D. Schurig, J. J. Mock, B. J. Justice, S. A. Cummer, J. B. Pendry, A. F. Starr, and D. R. Smith, "Metamaterial Electromagnetic Cloak at Microwave Frequencies," *Science* 314, 977 (2006).
9. R. Sun, F. Sun, and Y. Liu, "Research progress and development trend of electromagnetic cloaking," *Opto-Electron. Eng.* 51, 240191 (2024).
10. B. Zhang, "Electrodynamics of transformation-based invisibility cloaking," *Light:Sci. Appl.* 1, e32 (2012).
11. L. Xu, Q.-N. Wu, Y.-Y. Zhou, and H.-Y. Chen, "Transformation devices with optical nihility media and reduced realizations," *Front. Phys.* 14, 42501 (2019).
12. N. Landy and D. R. Smith, "A full-parameter unidirectional metamaterial cloak for microwaves," *Nat. Mater.* 12, 25 (2013).
13. Y. Zhang, Y. Luo, J. B. Pendry, and B. Zhang, "Transformation-Invariant Metamaterials," *Phys. Rev. Lett.* 123, 067701 (2019).
14. U. Leonhardt, "Optical Conformal Mapping," *Science* 312, 1777 (2006).
15. U. Leonhardt and T. Tyc, "Broadband Invisibility by Non-Euclidean Cloaking," *Science* 323, 110 (2009).
16. L. Xu and H. Chen, "Conformal transformation optics," *Nat. Photonics* 9, 15 (2015).
17. A. Alù and N. Engheta, "Plasmonic materials in transparency and cloaking problems: mechanism, robustness, and physical insights," *Opt. Express* 15, 3318 (2007).
18. A. Alù and N. Engheta, "Multifrequency Optical Invisibility Cloak with Layered Plasmonic Shells," *Phys. Rev. Lett.* 100, 113901 (2008).
19. A. Alù, "Mantle cloak: Invisibility induced by a surface," *Phys. Rev. B* 80, 245115 (2009).
20. J. Soric, Y. Ra'idi, D. Farfan, and A. Alù, "Radio-transparent dipole antenna based on a metasurface cloak," *Nat. Commun.* 13, 1114 (2022).
21. B. Zheng, Y. Yang, Z. Shao, Q. Yan, N.-H. Shen, L. Shen, H. Wang, E. Li, C. M. Soukoulis, and H. Chen, "Experimental Realization of an Extreme-Parameter Omnidirectional Cloak," *Research* 2019, 8282641 (2019).
22. Y. Gao, Y. Luo, J. Zhang, Z. Huang, B. Zheng, H. Chen, and D. Ye, "Full-parameter omnidirectional transformation optical devices," *Natl. Sci. Rev.* 11, nwad171 (2024).
23. X. Hu, Y. Luo, J. Wang, J. Tang, Y. Gao, J. Ren, H. Yu, J. Zhang, and D. Ye, "Multiband Omnidirectional Invisibility Cloak," *Adv. Sci.* 11, 2401295 (2024).
24. F. Sun, Y. Liu, and S. He, "Surface transformation multi-physics for controlling electromagnetic and acoustic waves simultaneously," *Opt. Express* 28, 94 (2019).
25. F. Sun, Y. Zhang, J. Evans, and S. He, "A camouflage device without metamaterials," *Prog. Electromagn. Res.* 165, 107 (2019).
26. R. Liu, C. Ji, J. J. Mock, J. Y. Chin, T. J. Cui, and D. R. Smith, "Broadband Ground-Plane Cloak," *Science* 323, 366 (2009).
27. J. Li and J. B. Pendry, "Hiding under the Carpet: A New Strategy for Cloaking," *Phys. Rev. Lett.* 101, 203901 (2008).
28. H. F. Ma and T. J. Cui, "Three-dimensional broadband ground-plane cloak made of metamaterials," *Nat. Commun.* 1, 21 (2010).
29. S. J. Penn, N. McN. Alford, A. Templeton, X. Wang, M. Xu, M. Reece, and K. Schrapel, "Effect of Porosity and Grain Size on the Microwave Dielectric Properties of Sintered Alumina," *J. Am. Ceram. Soc.* 80, 1885 (1997).